Journal of Solid State Chemistry 187 (2012) 114–123

Contents lists available at SciVerse ScienceDirect

Journal of Solid State Chemistry

journal homepage: www.elsevier.com/locate/jssc

The system Ta–V–Si: Crystal structure and phase equilibria

A.U. Khan [a], P. Broz [b,c], H.Y. Niu [d], J. Bursik [e], A. Grytsiv [a], X.-Q. Chen [d], G. Giester [f], P. Rogl [a,*]

[a] Institute of Physical Chemistry, University of Vienna, Währingerstrasse 42, A-1090 Wien, Austria
[b] Masaryk University, Department of Chemistry, Kolarska 2, 611 37, Brno, Czech Republic
[c] Masaryk University, Central European Institute of Technology, CEITEC, Kamenice 753/5, 625 00, Brno, Czech Republic
[d] Shenyang National Laboratory for Materials Science, Institute of Metal Research, Chinese Academy of Sciences, Shenyang, China
[e] Institute of Physics of Materials, Academy of Sciences of the Czech Republic, Zizkova 22, 61662 Brno, Czech Republic
[f] Institute of Mineralogy and Crystallography, University of Vienna, Althanstrasse 14, A-1090 Wien, Austria

ARTICLE INFO

Article history:
Received 22 October 2011
Received in revised form
10 December 2011
Accepted 18 December 2011
Available online 24 December 2011

Keywords:
Ternary alloy system
Microstructure
Phase diagram
Crystal structures

ABSTRACT

Phase relations have been evaluated for the Ta–V–Si system at 1500 and 1200 °C. Three ternary phases were found: τ_1-(Ta,V)$_5$Si$_3$ (Mn_5Si_3-type), τ_2-Ta(Ta,V,Si)$_2$ ($MgZn_2$-type) and τ_3-Ta(Ta,V,Si)$_2$ ($MgCu_2$-type). The crystal structure of τ_2-Ta(Ta,V,Si)$_2$ was solved by X-ray single crystal diffraction (space group $P6_3/mmc$). Atom order in the crystal structures of τ_1-(Ta,V)$_5$Si$_3$ (Mn_5Si_3 type) and τ_3-Ta(Ta,V,Si)$_2$ was derived from X-ray powder diffraction data. A large homogeneity range was found for τ_1-$(Ta_xV_{1-x})_5Si_3$ revealing random exchange of Ta and V at a constant Si content. At 1500 °C, the end points of the τ_1-phase solution ($0.082 \le x \le 0.624$) are in equilibrium with the solutions $(Ta_{1-x}V_x)_5Si_3$ (Cr_5B_3 type, $0 \le x \le 0.128$) and $(Ta_xV_{1-x})_5Si_3$ (W_5Si_3 type, $0 \le x \le 0.048$).

1. Introduction

Tantalum and vanadium are important constituents in martensitic steels for fusion reactors, which besides good thermal stability show low induced activity under neutron irradiation (low activation steels) [1,2]. With small amounts of Si in steels also the ternary system Ta–V–Si deserves attention, particularly as silicon is believed to be responsible for the stabilization of numerous complex phases in transition metal systems [3], including Laves phases. Information on phases and equilibria in the Ta–V–Si system has been collected by several research groups. As part of a study of the interaction of small non-metal atoms (B,C,N,O) with transition metal rich silicides, Nowotny et al. [4] presented a tentative phase field triangulation for the Ta–V–Si system at 1400 °C, which indicated two continuous solid solutions $(Ta_xV_{1-x})Si_2$ [5] and $(Ta_xV_{1-x})_5Si_3$, but did not reveal any ternary phase. It was stated that the small amounts of carbon, introduced by the vanadium metal pieces (containing 0.1 mass% C), are responsible to stabilize the complete solid solution $(Ta_xV_{1-x})_5Si_3$ with Mn_5Si_3-type, which has neither been observed at this temperature for pure Ta_5Si_3 (Cr_5B_3-type) [4] nor for pure V_5Si_3 (W_5Si_3-type) [6]. Although the isothermal section was clearly labeled by Nowotny et al. [4] to contain small amounts of carbon (actually as part of a quaternary system), a later report by English [7] dropped this information and quoting English a "carbon-free" phase diagram was republished in the ASM Handbook "Ternary Alloys" [8]. Later, Ganglberger et al. [9] and Mittal et al. [10] reported a ternary $MgZn_2$ type Laves phase, Ta_2V_3Si. A further ternary phase $Ta_{1.5}V_{3.5}Si_3$ with Mn_5Si_3 type was characterized by Steinmetz and Roques [11] and in a second article, another ternary phase $Ta_2V_4Si_5$ [12] was defined as part of a solid solution starting from binary V_6Si_5. A linear lattice parameter dependence on the Ta-content was derived for the solution $(Ta_xV_{1-x})_3Si$ at 1650 °C ($0 \le x \le 0.13$) [13].

All these partially contradicting information demand on a renewed study of the phase relations in the Ta–V–Si system under pure conditions. Furthermore, there is a lack of complete structure determinations for the ternary Laves and Mn_5Si_3 type structures. Therefore, the present investigation intends to provide a comprehensive evaluation of the equilibria and crystal structures for ternary phases in the Ta–V–Si system.

2. Experimental details

Alloys were prepared (each of 1–2 g) by arc melting from metal ingots of Ta, V and pieces of Si all with purity higher than 99.9 mass% (Alfa Johnson Matthey GmbH, Germany) and were melted three times under 6N argon for homogenization on a water cooled copper plate (weight loss less than 0.1%). As-cast alloys were annealed on an Al_2O_3 support for 7–15 days at 1500 °C and subsequently at 1200 °C (for 7–15 days) in a high

* Corresponding author.
E-mail address: peter.franz.rogl@univie.ac.at (P. Rogl).

0022-4596/$ - see front matter © 2011 Elsevier Inc. All rights reserved.
doi:10.1016/j.jssc.2011.12.024

vacuum furnace at 3×10^{-4} Pa with a W-sheet metal heater and then were radiation cooled by cutting the power to the W-heater. There was no reaction between support and samples. In many cases, it was difficult to get equilibrium even after 10 days of annealing at 1500 °C. So repeated grinding (in a WC-mortar), compacting (in steel dies without lubricants) and annealing of samples served to attain equilibrium. Lattice parameters and standard deviations were determined by least squares refinements of room temperature X-ray powder diffraction (XPD) data obtained from a Guinier-Huber image plate employing monochromatic Cu $K\alpha_1$ radiation with Ge as internal standard. Samples were polished using standard procedures and were examined by optical metallography and scanning electron microscopy (SEM). Composition of particular phases was measured using a JEOL JSM 6460 scanning electron microscope equipped with both energy- and wavelength dispersive X-ray analytical systems INCA Energy and INCA Wave by Oxford Instruments. An acceleration voltage of 20 kV was used. Reliable evaluation of the Si content in the Ta–V–Si alloys is hindered by a strong overlap of the Si K_α peak at 1.740 keV and the Ta M_α peak at 1.710 keV in energy dispersive X-ray (EDX) spectra. Thus, wavelength dispersive X-ray analysis (WDX) with well-separated wavelengths needs to be used for accurate composition measurements. Si K_α, V K_α and Ta L_α were used for quantification at an electron beam current of about 15 nA. The full width at half maximum of the Si K_α peak measured experimentally in WDX is only about 2 eV, hence no overlap with the Ta M_α peak at 1.710 keV can occur. Pure elements served as standards to quantify. Finally, the X-ray intensities were corrected for ZAF effects. Single crystals of τ_2-Ta(Ta,V,Si)$_2$ ($MgZn_2$-type Laves phase) suitable for X-ray diffraction were mechanically isolated from an arc-melted specimen $Ta_{33.3}V_{50}Si_{16.7}$ (nominal composition in at.%) that was annealed at 1500 °C for 10 days. The crystals were inspected on an AXS-GADDS texture goniometer for quality and crystal symmetry prior to X-ray intensity data collection on a four-circle Nonius Kappa diffractometer (CCD area detector and graphite monochromated Mo K_α radiation, $\lambda = 0.071069$ nm). Orientation matrix and unit cell parameters were derived using the program DENZO [14]. No absorption correction was necessary because of the rather regular crystal shape and small dimensions of the investigated specimen ($30 \times 30 \times 35$ μm^3). The structure was solved by direct methods and refined with the SHELXS-97 and SHELXL-97 programs [15], respectively.

3. Results and discussion

3.1. Binary boundary systems

Some controversy exists for the Ta–V binary phase diagram. The critical assessment in Massalski [16] shows a continuous bcc-type solid solution (Ta,V) at high temperatures and a binary Laves phase with $MgCu_2$ structure (C15) below a critical point at 1310 °C. In contrast to the version by Massalski, which is backed by four out of five independent investigations [17–20] Savitskii and Efimov [21] reported the additional formation of a hexagonal Laves phase with $MgZn_2$-type (C14) in a limited temperature range from 1125 to 1430 °C and this phase was included in the binary phase diagram as a high temperature modification of low temperature TaV_2 with $MgCu_2$-type. The most recent attempts for a thermodynamic modeling of the Ta-V binary system by Pavlu et al. [22], and a similar assessment by Canon and Servant [23], relied on the phase relations given by Savitskii and Efimov [21]. In the present investigation, we could not confirm the hexagonal Laves phase in the binary Ta–V system in samples annealed at 1200 °C for 15 days. Fig. 1 summarizes all the various versions of the binary Ta–V phase diagram, that have hitherto been published in the literature [16–21]. The data points obtained from our investigation of the two-phase regions at 1200 °C between the $MgCu_2$-type phase and bcc-(Ta,V) reveal the best correspondence with data published by Rudy [20] for the bcc-phase limits and with the data by Nefedov [17] for the extent of the homogeneity region of the cubic Laves phase (32.9–36.5, at.% Ta). For the Ta–Si system, we accept the thermodynamic assessment of Guo et al. [24]. A thermodynamic modeling of the system V–Si is due to Zhang et al. [25], reviewed by Okamoto [26]. It should be

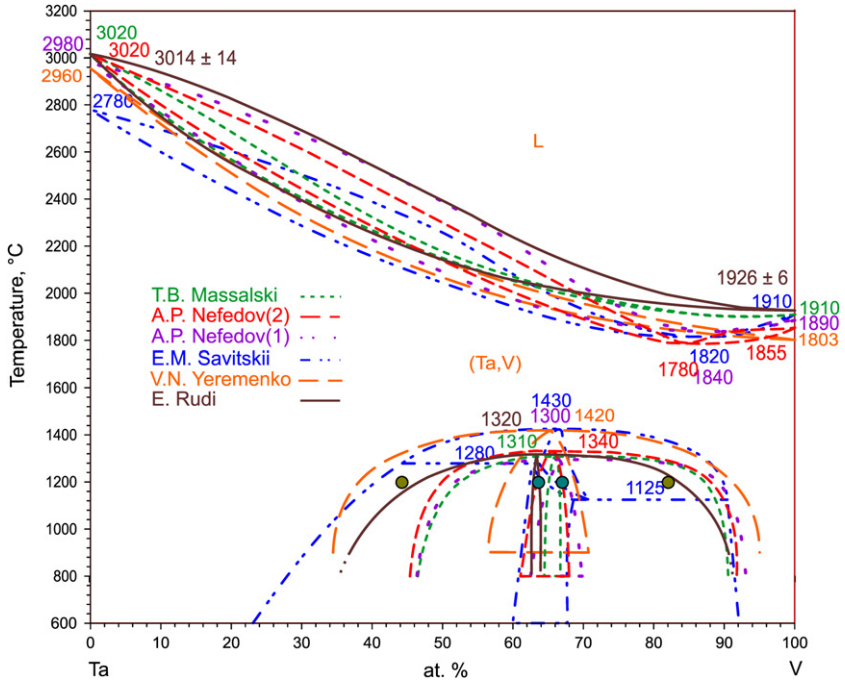

Fig. 1. Ta–V binary phase diagrams based on experimental data [16–21]. Circles represent the phase equilibria obtained in the present work at 1200 °C.

emphasized, that although the Nb_6Sn_5 type structure (space group *Immm*) was assigned by Hallais et al. [27] to the V_6Si_5-phase, V_6Si_5, however, adopts its own structure type (space group *Ibam*), as derived from single crystal X-ray data presented by Spinat et al. [28] and Hallais [29]. All crystal data on solid unary and binary phases pertinent to the Ta–V–Si system are summarized in Table 1.

3.2. Crystal structure of τ_2-Ta(Ta,V,Si)$_2$ ($MgZn_2$-type laves phase)

A ternary compound with the $MgZn_2$-type structure was reported by Ganglberger et al. [9] and Mittal et al. [10] at 1000 °C to be present in a sample with the nominal composition Ta_2V_3Si for which Mittal et al. [10] also reported small amounts of secondary phases. However, only the lattice parameters were published for this phase. Our sample with composition Ta_2V_3Si annealed at 1500 °C turned out to be three-phase as it contains the $MgZn_2$-type phase as the main constituent but in addition smaller amounts of τ_1-$(Ta_xV_{1-x})_5Si_3$ ($x=0.539$, Mn_5Si_3 type) and $(Ta_xV_{1-x})_3Si$ ($x=0.091$) as secondary phases. Lattice parameters for the Laves phase (labeled τ_2, $a=0.50158(2)$, $c=0.82642(3)$ nm), however, are close to the values given by Ganglberger et al. [9] [$a=0.500$, $c=0.826$ nm] and Mittal et al. [10] [$a=0.505$, $c=0.823$ nm].

Systematic extinctions for a single crystal selected from this sample prompted the space group types $P6_3/mmc$, $P\text{-}62c$ and $P6_3mc$. As practically identical solutions were found, we describe the structure in the space group with highest symmetry $P6_3/mmc$ (194). Structure solution via direct methods prompts a full occupation of sites 4*f* and 6*h* by Ta and V, respectively. Atom displacement parameters (ADP's) for site 2*a*, however, indicate a statistical mixture. A random mixture of only two atoms (V and Si) on this site resulted in a significant deviation of the composition by a deficiency of about 4 at.% Si from the EPMA data. This simple model could furthermore not explain the homogeneity region of the τ_2-phase revealing a Ta content of more than 33.3 at.%, which clearly suggested that Ta should be present at sites 2*a* or 6*h* in addition to the 4*f* site. Ta in site 6*h* was not accepted by the refinement. However, when Ta was introduced to the 2*a* site, the amount of Si

Table 1
Crystallographic data of solid phases in the Ta–V–Si system.

Phase temperature range (°C)	Space group prototype	Lattice parameters (nm)			Comments
		a	b	c	
$(Ta_{1-x}V_x)$	*Im*-3*m*	0.3305-			[30,20] (see Fig. 6)
	W	0.3325			
(Ta); < 3020 [16]		0.33030			[16]
(V); < 1910 [16]		0.3024			[16]
$(V_{1-x}Si_x)$		0.30232-			$0 < x < 0.03$ [31]
		0.303			
(Si)	*Fd*-3*m*	0.54306			[16]
< 1414 [16]	C (diamond)				
TaV_2	*Fd*-3*m*	0.7157			[32]
≤ 1310 [16]	$MgCu_2$				
TaV_2	$P6_3/mmc$	0.5058(5)		0.8250(5)	[17]
1435–1127 and ≤ 370 [this work]	$MgZn_2$				
$(Ta_{1-x}V_x)_3Si$	$P4_2/n$	1.00903(9)		0.51276(9)	$x^1_{max}=0.160$, [this work]
	Ti_3P				$0 \le x \le 0.160$, [this work]
Ta_3Si; < 2340 [24]		1.0184		0.5183	[33]
$(Ta_{1-x}V_x)_2Si$	*I*4/*mcm*	0.61454(7)		0.50431(7)	$x^1_{max}=0.123$, [this work]
	$CuAl_2$	0.61623(8)		0.50574(7)	$x=0$, [this work]
Ta_2Si; < 2440 [24]		0.6172		0.505	[33]
$(Ta_{1-x}V_x)_5Si_3$	*I*4/*mcm*	0.64430(7)		1.19154(9)	$x^1_{max}=0.128$, [this work]
	Cr_5B_3	0.65154(5)		1.18753(9)	$x=0$, [this work]
Ta_5Si_3; < 2160 [24]		0.6519		1.187	[33]
$(Ta_{1-x}V_x)Si_2$	$P6_222$	0.4574-		0.6357-	$0 < x < 1$, graph given
	$CrSi_2$	0.4766		0.6549	Annealed at 1300 °C [30]
$TaSi_2$; < 2034 [24]		0.4784		0.6568	[34]
VSi_2; < 1683 [25]		0.4573		0.6374	[34]
$(Ta_xV_{1-x})_3Si$	*Pm*-3*n*	0.4755(4)			$x^1_{max}=0.086$, [this work]
	Cr_3Si	0.4763			$x_{max}=0.13$ at 1650 °C [13]
V_3Si; < 1921 [25]		0.4725			$x=0$, [13]
		0.4727			[35]
$(Ta_xV_{1-x})_5Si_3$	*I*4/*mcm*	0.94674(7)		0.47752(6)	$x=0.048$, [this work]
V_5Si_3	W_5Si_3	0.94264(4)		0.47585(3)	$x=0$, [this work]
< 1987 [25]		0.9383		0.4760	[36]
Ta_5Si_3		0.9892		0.5042	[33]
2543–2160 [24]					
V_6Si_5	Immm	0.4858	1.5966	0.7501	[27] Incorrect structure type
1667–459 [25]	Nb_6Sn_5				
$(Ta_xV_{1-x})_6Si_5$	Ibam	0.7625(5)	1.609(1)	0.4936(3)	$x_{1200\ °C}=0.333$ [12]
	V_6Si_5	0.7643(7)	1.6078(5)	0.4939(5)	$x^1_{max}=0.367$, [this work]
V_6Si_5		0.7501	1.5966	0.4858	$x=0$, [28]
1667–459 [25]		0.7501	1.5966	0.4858	$x=0$, [29]
τ_1-$(Ta_xV_{1-x})_5Si_3$	$P6_3/mcm$	0.7258(6)		0.4926(3)	$Ta_{1.5}V_{3.5}Si_3$ [10]
	Mn_5Si_3	0.71976-		0.48906-	$0.0816 \le x_{1500\ °C} \le 0.624$
		0.73914		0.50135	
τ_2-$Ta(Ta_xV_{1-x-y}Si_y)_2$	$P6_3/mmc$	0.500(3)		0.826(0)	[9], for "Ta_2V_3Si"
	$MgZn_2$	0.505		0.823	Annealed at 1000 °C [10]
τ_3-$Ta(Ta_xV_{1-x-y}Si_y)_2$	*Fd*-3*m*	0.71510(1)			Annealed at 1500 °C [this work]
	$MgCu_2$				

[a]Maximal solubility at 1500 °C.

Table 2a
X-ray single crystal data for τ_2-$Ta_2V_3(Ta_{0.034}V_{0.228}Si_{0.738})$, $2^\circ \le 2\theta \le 70^\circ$; ω-scans, scan width 2°, 150 s/frame and results of Rietveld refinement of τ_1 and τ_3. All structures are standardized with program Structure Tidy [37]. Anisotropic displacement parameters are in 10^2 nm^2.

Parameter/compound	τ_1	τ_2	τ_3
Method	XPD (Cu Kα1)	XSC (Mo Kα)	XPD (Cu Kα1)
Structure type	Mn_5Si_3	$MgZn_2$	$MgCu_2$
Space group	$P6_3/mcm$, #193	$P6_3/mmc$, #194	Fd-3m, #227
Composition from EPMA	$Ta_{19.0}V_{43.5}Si_{37.5}$[a]	$Ta_{34.4}V_{53.3}Si_{12.3}$	$Ta_{36.1}V_{60.0}Si_{3.9}$
Composition from refinement	$Ta_{18.0}V_{44.5}Si_{37.5}$	$Ta_{33.9}V_{53.8}Si_{12.3}$	$Ta_{36.3}V_{59.8}Si_{3.9}$
Formula from refinement	$(Ta_xV_{1-x})_5Si_3$, $x=0.288$	$Ta(Ta_xV_{1-x-y}Si_y)_2$, $x=0.009$, $y=0.184$	$Ta(Ta_xV_{1-x-y}Si_y)_2$, $x=0.022$, $y=0.030$
a (nm)	0.72545(2)	0.50158(2)	0.71510(1)
b (nm)	0.72545(2)	0.50158(2)	0.71510(1)
c (nm)	0.49259(1)	0.82642(3)	0.71510(1)
Reflections in refinement	60	$188 \ge 4\sigma(F_o)$ of 195	18
Mosaicity	–	0.51	–
Number of variables	19	16	19
$R_F=\Sigma\lvert F_0-F_c\rvert/\Sigma F_0$	0.033	–	0.058
$R_I=\Sigma\lvert I_0-I_c\rvert/\Sigma I_0$	0.029	–	0.038
$R_{wP}=[\Sigma w_i\lvert y_{0i}-y_{ci}\rvert^2/\Sigma w_i\lvert y_{0i}\rvert^2]^{1/2}$	0.032	–	0.046
$R_P=\Sigma\lvert y_{0i}-y_{ci}\rvert/\Sigma\lvert y_{0i}\rvert$	0.025	–	0.035
$R_e=[(N-P+C)/\Sigma w_i y_{0i}^2]^{1/2}$	0.013	–	0.021
$\chi^2=(R_{wp}/R_e)^2$	7.76	–	4.80
$R_F^2=\Sigma\lvert F_0^2-F_c^2\rvert/\Sigma F_0^2$	–	0.015	–
R_{Int}	–	0.016	–
wR2	–	0.035	–
GOF	–	1.204	–
Extinction (Zachariasen)	–	0.0037(6)	–
Residual density e$^-$/Å^3; max; min.	–	1.36; −1.40	–
Atom parameters			
Atom site 1	4d (1/3, 2/3, 0);	2a (0, 0, 0);	8b (3/8, 3/8, 3/8);
Occ.	1.00 V	0.033(4) Ta +0.226 V+0.741 Si[b]	1.00 Ta
$U_{11}=U_{22}$; U_{33}	–	0.0050(7); 0.0052(9)	–
$U_{23}=U_{13}=0$, U_{12}	B_{iso}=0.653(7)	0.0025(4)	B_{iso}=0.693(2)
Atom site 2	6g (x, 0, ¼)	4f ($^1/_3$, $^2/_3$, z)	16c (0, 0, 0)
Occ.	0.48(3) Ta + 0.52 V	1.00 Ta	0.044(3) Ta +0.897 V +0.059 Si[b]
x, z;	x=0.23805(6)	z=0.56126(4)	–
$U_{11}=U_{22}$; U_{33}	–	0.0045(1); 0.0039(1)	–
$U_{23}=U_{13}=0$, U_{12}	B_{iso}=0.714(9)	0.0023(1)	B_{iso}=0.621(9)
Atom site 3	6g (x, 0, ¼);	6h (x, 2x, ¼);	–
Occ.	1.00 Si	1.00 V	–
x;	0.5943(2)	0.1707(1)	–
U_{11}; U_{22}; U_{33}	–	0.0040(3); 0.0030(4)	–
$U_{23}=U_{13}=0$, U_{12}	B_{iso}=0.725(6)	0.0015(2)	–

[a]Composition from graph in Fig. 5.
[b]Si content fixed after EPMA.

Table 2b
Interatomic distances (nm) for $Ta_2V_3(Ta_{0.034}V_{0.228}Si_{0.738})$ from XSC. Standard deviation ≤0.0001.

Ta−	−3V	0.2935		−1Ta	0.3120		−2Ta	0.2935
CN=16	−3M	0.2940	V−	−2V	0.2448		−4Ta	0.2954
	−6V	0.2954	CN=12	−2M	0.2543	M−	−6V	0.2543
	−3Ta	0.3068		−2V	0.2568	CN=12	−6Ta	0.2940

increased. Therefore, we fixed the Si content in this site according to the EPMA data and refined the occupation of Ta and V. The final composition from single crystal refinement, $Ta_{33.9}V_{53.8}Si_{12.3}$, is in good agreement with EPMA ($Ta_{34.4}V_{53.3}Si_{12.3}$). Tables 2a and 2b comprises the results of the single crystal refinement with a final R-factor R_{F2}=0.015 and negligible residual electron densities (1.36, −1.40 e$^-$/Å^3). The structure solution obtained, $Ta_2V_3(Ta,V,Si)_1$, fits well with the X-ray powder diffraction data. Fig. 2 presents the coordination polyhedra for the τ_2-phase.

3.3. Rietveld refinements of τ_3-$Ta(Ta_xV_{1-x-y}Si_y)_2$ ($MgCu_2$-type) and τ_1-$(Ta_xV_{1-x})_5Si_3$ (Mn_5Si_3-type)

Detailed inspection of the phase equilibria at 1500 °C revealed a Laves phase with $MgCu_2$ type (τ_3-phase). The Rietveld refinement of the X-ray powder spectrum of the alloy $Ta_{36.1}V_{60.0}Si_{3.9}$ (EPMA, at.%) in Fig. 3 confirms the τ_3-phase in equilibrium with the solid solution (Ta,V) and with traces of τ_2. The refinement shows that the 8b site is fully occupied by Ta only, whilst the 16c site is shared by all three elements Ta, V and Si (Tables 2a and 2b). Thus, the Si content was fixed to comply with the EPMA data, and Ta and V amounts were refined for this site. Convergence was achieved at an R-value of R_F=0.033. Compositions obtained from the refinement ($Ta_{36.3}V_{59.8}Si_{3.9}$) and from EPMA ($Ta_{36.1}V_{60.0}Si_{3.9}$) are in good agreement with each other.

X-ray intensities of a powder spectrum of $(Ta_{0.3}V_{0.7})_5Si_3$, a ternary compound with Mn_5Si_3 type, were reported by Steinmetz and Roques [11] to be consistent with a statistical mixture of 3 Ta and 3 V atoms sharing the 6g position, however, no further structural details were given. Our Rietveld X-ray powder data refinement (see Fig. 4) of a sample with composition $Ta_{20}V_{40}Si_{40}$ [τ_1-phase; $(Ta_{0.3}V_{0.7})_5Si_3$] confirmed the Mn_5Si_3 type as well as the preferred partial occupation of the 6g-site by Ta-atoms. Mn_5Si_3 type phases are known to be stabilized by various impurities (B, C, O, etc.) and therefore were frequently observed in Ta–Si and V–Si binary systems by several research groups [38–41]. In the present study, we did not encounter this phase in binary samples, however, the τ_1-$(Ta_xV_{1-x})_5Si_3$ phase with Mn_5Si_3 type was clearly received in ternary alloys. Rietveld refinement of

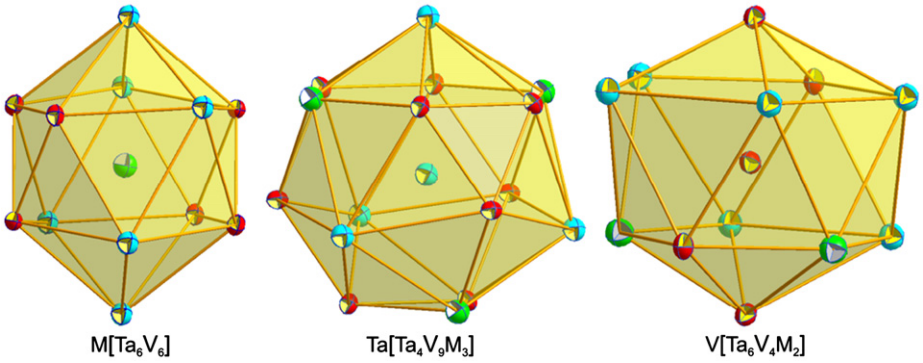

Fig. 2. Coordination polyhedra of τ_2-Ta(TaVSi)$_2$ showing atoms with anisotropic displacement parameters from X-ray single crystal refinement. Green (gray in black and white) shows the mixed position occupied by Ta, V and Si atoms; blue (white in black and white) represents Ta atoms and red (black in black and white) represents V atoms. (For interpretation of the reference to color in this figure legend the reader is referred to the web version of this article.)

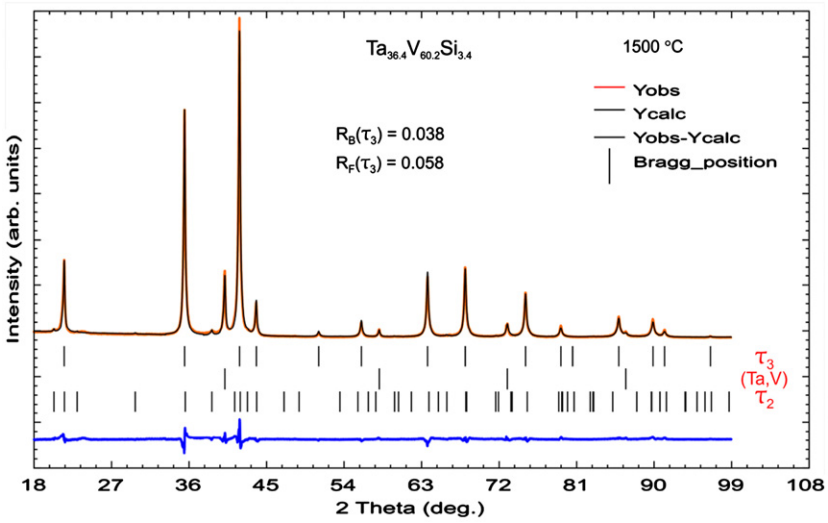

Fig. 3. Refinement of $Ta_{36.4}V_{60.2}Si_{3.4}$ (alloy annealed at 1500 °C; composition from EPMA in at.%); equilibrium between τ_3-($Ta_{36.1}V_{60.0}Si_{3.9}$)+($Ta_{50.3}V_{49.7}$)+$\tau_2$ (traces).

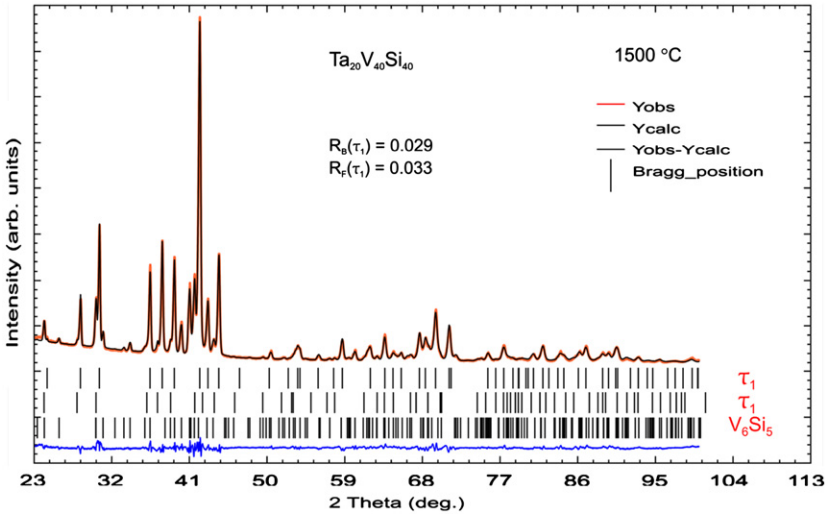

Fig. 4. Refinement of $Ta_{20}V_{40}Si_{40}$ (alloy annealed at 1500 °C after repeated grinding and compacting, composition in at.%). τ_1-phase shows two lattice parameters due to initial inhomogeneity of the as cast sample, which did not disappear even after repeated grinding, compacting and annealing.

the τ_1-phase; $(Ta_{0.3}V_{0.7})_5Si_3$ did not reveal any significant residual electron density in the sites for the octahedral voids in 2*b* (0, 0, 0) excluding contamination. Furthermore, the interatomic distances from the center of these voids are unfavorable for the incorporation of Si/V atoms ($d_{2b-\text{metal}}$=0.212153 nm) in terms of a Ti_5Ga_4-type [42] and EPMA for this phase measured on various alloys confirms the metal/Si ratio $(Ta_xV_{1-x})_5Si_3$ ±1 at.%. It can, thus, be safely assumed that the τ_1-$(Ta_xV_{1-x})_5Si_3$ phase is a truly ternary phase with stoichiometry M_5Si_3. Tables 2a and 2b summarizes the structural parameters for τ_1-$(Ta_{0.3}V_{0.7})_5Si_3$.

The τ_1-phase exhibits a large homogeneity region extending at 1500 °C from $Ta_{5.1}V_{57.4}Si_{37.5}$ (at.%) to $Ta_{39.0}V_{23.5}Si_{37.5}$ (at.%). It is interesting to note that the Ta-rich solubility limit at 1500 °C practically coincides with a full occupation of Ta in the 6*g* site yielding the ordered composition $Ta_3V_2Si_3$ ($Ta_{37.5}V_{25}Si_{37.5}$, at.%). However, the amount of Ta for this phase in the as cast samples exceeds the stoichiometric limit for a fully ordered composition $Ta_3V_2Si_3$. Refinement for alloys on the Ta-rich side of the homogeneity region showed Ta entering the 4*d* site after complete replacement of V by Ta in the 6*g* site.

3.4. Isothermal section of the Ta–V–Si system at 1500 °C

Although the $MgCu_2$ type Laves phase is not present in the Ta–V binary system at 1500 °C, it was observed in the Ta–V–Si ternary at this temperature with a rather small homogeneity range (~3–4 at.% Si content and 1–2 at.% Ta/V exchange). This phase (τ_3) is clearly separated from the binary system revealing a two-phase equilibrium with the Si-saturated solid solution of (Ta,V). In view of the existence of binary TaV_2 with $MgCu_2$-type below about ~1320 °C, the small amounts of Si are conceived to significantly increase the stability of the cubic Laves phase.

Ganglberger et al. [9] and Mittal et al. [10] reported the composition Ta_2V_3Si for the τ_2-phase with $MgZn_2$-type at 1000 °C. At 1500 °C, we observed τ_2 with a considerable homogeneity region from ~8 to 12 at.% Si and from ~34 to 37 at.% Ta, however, excluding the stoichiometric composition Ta_2V_3Si.

At 1500 °C τ_1-$(Ta_xV_{1-x})_5Si_3$ exists in a large homogeneity region extending from $Ta_{5.1}V_{57.4}Si_{37.5}$ ($x=0.064$) to $Ta_{39}V_{23.5}Si_{37.5}$ ($x=0.624$). The compositional dependences for the average volume per atom for the solutions along the isopleth Ta_5Si_3–V_5Si_3 with Mn_5Si_3-, W_5Si_3- and Cr_5B_3-types show almost linear dependence (Fig. 5) and agree well with the data of Steinmetz and Roques [11] for τ_1-$(Ta_{0.3}V_{0.7})_5Si_3$ (Mn_5Si_3-type).

Lattice parameters as a function of composition for binary (Ta_xV_{1-x}) and ternary ($Ta_xV_{1-x-y}Si_y$) are presented in Fig. 6. Literature data for binary (Ta_xV_{1-x}) [24,27] are close to lattice parameters determined for the ternary Si-saturated (Ta,V)-solid solution ($Ta_xV_{1-x-y}Si_y$). The dependences (Figs. 5 and 6) are used to determine the composition of the phases via their lattice parameters in those samples for which EPMA was difficult to perform (powdered and sintered samples) and thereby help to define the extent of the three solid solutions in the isopleth Ta_5Si_3–V_5Si_3.

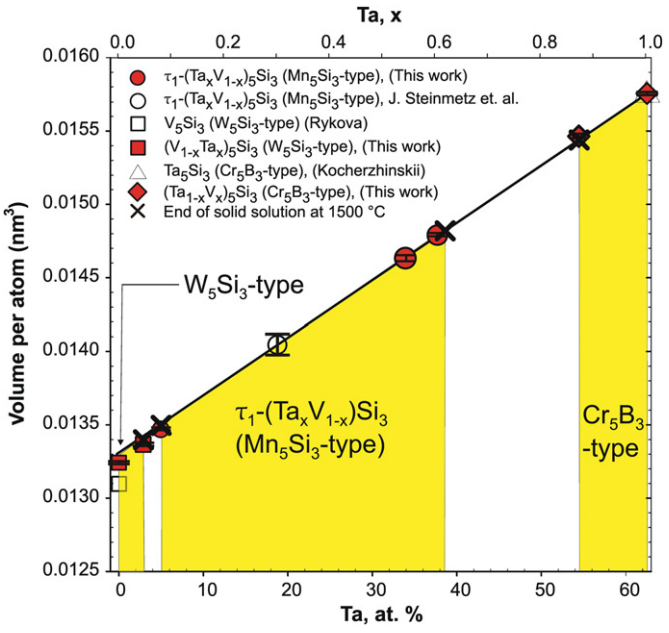

Fig. 5. Volume per atom (nm^3) vs composition for the section $(Ta_xV_{1-x})_5Si_3$. Data for τ_1-$(Ta_xV_{1-x})_5Si_3$ (Mn_5Si_3 type) given by Steinmetz and Roques [11], for Ta_5Si_3 (Cr_5B_3-type) given by Kocherzhinskii et al. [33] and for binary V_5Si_3 (W_5Si_3-type) given by Rykova et al. [36] are also shown.

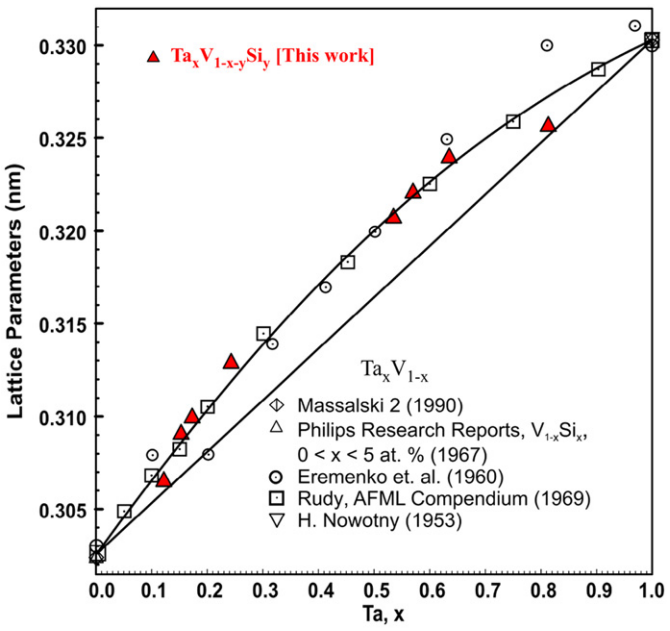

Fig. 6. Compositional dependence for lattice parameters of the ternary $Ta_xV_{1-x-y}Si_y$ and binary Ta_xV_{1-x} phase: filled symbols [this work] and open symbols from the literature [16,20,30,31,40].

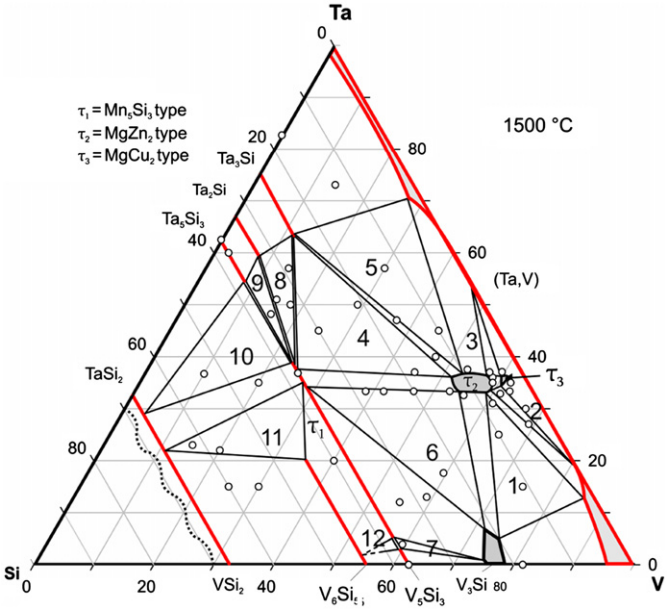

Fig. 7. Isothermal section of Ta–V–Si system at 1500 °C. Sample location is shown by open circles. Numbers in three-phase fields relate to the numbering in Table 3.

The continuous solid solution between $TaSi_2$ and VSi_2, reported by Nowotny et al. [5] at 1300 °C, is confirmed to exist at 1500 °C.

A phase with unknown structure type and with a composition ranging from $Ta_{47}V_{37}Si_{16}$ to $Ta_{49.5}V_{32.5}Si_{18}$ (at.%) was observed in as cast samples, but it disappears after continuous grinding,

compacting and annealing of these samples and thus is not present at 1500 °C.

Fig. 7 shows the isothermal section of the Ta–V–Si system at 1500 °C. Composition of vertices and the phases found in all triangles are summarized in Table 3. The numbering shown in the isothermal section in Fig. 7 corresponds to the same numbers for the three-phase regions listed in Table 3. Fig. 8a,b,c,d shows the micrographs of selected samples annealed at 1500 °C documenting the two-phase equilibria $\tau_2+(Ta_xV_{1-x})_3Si$ and $\tau_2+(Ta,V)$ as well as the three-phase equilibria $\tau_1+\tau_2+(Ta_xV_{1-x})_3Si$ and $\tau_2+\tau_3+(Ta,V)$. Equilibrium among $(Ta_xV_{1-x})_6Si_5+\tau_1+(Ta_{1-x}V_x)Si_2$ was finally achieved by continuous grinding, compacting and annealing. Due to the impossibility to employ EPMA on sinter-bodies, the compositions at the vertices of the three-phase equilibrium were defined via lattice parameters using the graph in Fig. 5 for τ_1 and the graph reported by Nowotny et al. [5] for $(Ta_{1-x}V_x)Si_2$. The composition of the $(V_{1-x}Ta_x)_6Si_5$ phase was reliably measured by EPMA along with the lattice parameters.

3.5. Isothermal section of the Ta–V–Si system at 1200 °C

Our main focus at 1200 °C was on the homogeneity region of the two Laves phases, τ_2 and τ_3, and their connection with the binary Ta–V system. Savitskii and Efimov [21] showed the presence of two corresponding binary Laves phases: TaV_2 with $MgCu_2$-type for the low-temperature form and with the $MgZn_2$-type for the high-temperature modification. The Ta–V phase diagram calculated by Pavlu et al. [22] refers to this data. However, we could not find any connection of τ_2 present in the ternary Ta–V–Si system with a corresponding isotypic binary Ta–V phase. In fact, our binary Ta,V-samples annealed at 1200 °C did not reveal any presence of the hT-$MgZn_2$-type Laves phase (see

Table 3
Data on alloys for three-phase regions in the Ta–V–Si system at 1500 °C.

Three phase regions	Phase	Structure type	Lattice parameters (nm)			Composition (at.%)		
			a	*b*	*c*	Ta	V	Si
$\tau_2+(Ta_xV_{1-x})_3Si$ + (Ta,V)	τ_2	$MgZn_2$	0.50215(6)	–	0.82102(4)	33.9	58.1	8.0
(1)[a]	$(Ta_xV_{1-x})_3Si$	Cr_3Si	0.47525(4)	–	–	4.5	75.1	20.4
	(Ta,V)	W	0.30656(5)	–	–	13.0	85.0	2.0
$\tau_2+\tau_3+(Ta,V)$	τ_2	$MgZn_2$	0.50321(6)	–	0.82668(8)	34.6	60.3	5.1
(2)	τ_3	$MgCu_2$	0.71279(2)	–	–	34.4	58.8	6.8
	(Ta,V)	W	0.30976(14)	–	–	18.4	80.3	1.3
$\tau_2+\tau_3+(Ta,V)$	τ_2	$MgZn_2$	0.50586(7)	–	0.82555(15)	37.8	57.2	5.0
(3)	τ_3	$MgCu_2$	0.71559(6)	–	–	37.5	58.3	4.2
	(Ta,V)	W	0.32076(6)	–	–	53.5	46.5	0.0
$\tau_1+\tau_2$ + $(Ta_xV_{1-x})_3Si$	τ_2	$MgZn_2$	0.50099(3)	–	0.82565(9)	34.5	53.0	12.5
(6)	τ_1	Mn_5Si_3	0.73615(5)	–	0.49888(6)	33.7	28.8	37.5
	$(Ta_xV_{1-x})_3Si$	Cr_3Si	0.47554(1)	–	–	6.8	71.9	21.3
$\tau_1+(Ta_xV_{1-x})_5Si_3$ + $(Ta_xV_{1-x})_3Si$	τ_1	Mn_5Si_3	0.71986(7)	–	0.48936(6)	5.1	57.4	37.5
(7)	$(Ta_xV_{1-x})_5Si_3$	W_5Si_3	0.94674(7)	–	0.47752(6)	3.0	59.5	37.5
	$(Ta_xV_{1-x})_3Si$	Cr_3Si	–	–	0.47285(3)	0.6	74.2	25.2
$\tau_2+(Ta_xV_{1-x})_3Si$ + (Ta,V)	τ_2	$MgZn_2$	0.50261(3)	–	0.82736(3)	37.1	52.8	10.1
(5)	$(Ta_{1-x}V_x)_3Si$	Ti_3P	1.01128(6)	–	0.51351(7)	63.0	12.0	25.0
	(Ta,V)	W	0.32340(1)	–	–	69.0	31.0	0.0
$\tau_1+\tau_2$ + $(Ta_{1-x}V_x)_3Si$	τ_1	Mn_5Si_3	0.73792(8)	–	0.50176(7)	37.7[b]	24.8	37.5
(4)	τ_2	$MgZn_2$	0.50171(7)	–	0.82587(6)	34.9	52.4	12.7
	$(Ta_{1-x}V_x)_3Si$	Ti_3P	1.00903(9)	–	0.51276(9)	63.0	12.0	25.0
$\tau_1+(Ta_{1-x}V_x)_2Si$ + $(Ta_{1-x}V_x)_3Si$	τ_1	Mn_5Si_3	0.73912(9)	–	0.50100(9)	38.4	24.1	37.5
(8)	$(Ta_{1-x}V_x)_2Si$	$CuAl_2$	0.61454(7)	–	0.50431(7)	58.5	8.2	33.3
	$(Ta_{1-x}V_x)_3Si$	Ti_3P	–	–	–	62.9	12.1	25.0
$\tau_1+(Ta_{1-x}V_x)_2Si$ +$(Ta_{1-x}V_x)_5Si_3$	τ_1	Mn_5Si_3	0.73914(7)	–	0.50135(9)	39.0[b]	23.5	37.5
(9)	$(Ta_{1-x}V_x)_2Si$	$CuAl_2$	0.61352(6)	–	0.50343(8)	58.6	8.1	33.3
	$(Ta_{1-x}V_x)_5Si_3$	Cr_5B_3	0.64430(7)	–	1.19154(9)	54.5[b]	8.0	37.5
$\tau_1+(Ta_{1-x}V_x)_5Si_3$ +$(Ta_{1-x}V_x)Si_2$	τ_1	Mn_5Si_3	0.73834(9)	–	0.50233(8)	38.6[b]	23.9	37.5
(10)	$(Ta_{1-x}V_x)_5Si_3$	Cr_5B_3	0.64308(6)	–	1.19042(8)	54.5[b]	8.0	37.5
	$(Ta_{1-x}V_x)Si_2$	$CrSi_2$	0.47585(3)	–	0.65492(9)	29.8[b]	3.5	66.7
$\tau_1+(Ta_xV_{1-x})_6Si_5$ + $(Ta_{1-x}V_x)Si_2$	τ_1	Mn_5Si_3	0.73781(7)	–	0.49995(6)	35.0[b]	27.5	37.5
(11)	$(Ta_xV_{1-x})_6Si_5$	V_6Si_5	0.76214(8)	1.60989(8)	0.49380(5)	20.0	35.0	45.0
	$(Ta_{1-x}V_x)Si_2$	$CrSi_2$	0.47202(8)	–	0.65125(7)	22.0[b]	11.3	66.7
$\tau_1+(Ta_xV_{1-x})_6Si_5$ +$(Ta_xV_{1-x})_5Si_3$	τ_1	Mn_5Si_3	0.71976(5)	–	0.48906(7)	5.1	57.4	37.5
(12)	$(Ta_xV_{1-x})_6Si_5$	V_6Si_5	–	–	–	2.5[c]	52.0	45.5
	$(Ta_xV_{1-x})_5Si_3$	W_5Si_3	0.94624(5)	–	0.47732(5)	3.0	59.5	37.5

[a] Corresponding no. of triangles shown in isothermal section at 1500 °C in Fig. 7.
[b] Composition of phases evaluated from Figs. 5 and 6.
[c] Estimated value for triangle, which is dotted in the isothermal section at 1500 °C.

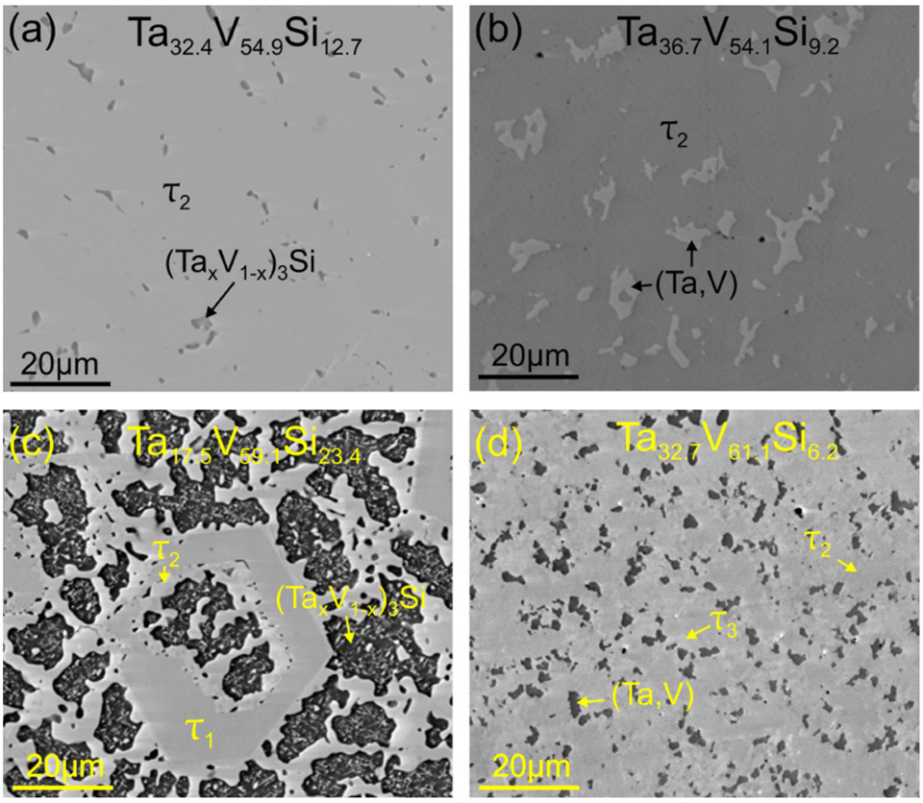

Fig. 8. Micrographs of selected samples annealed at 1500 °C. (a) $Ta_{32.4}V_{54.9}Si_{12.7}$; $\tau_2+(Ta_xV_{1-x})_3Si$, (b) $Ta_{36.7}V_{54.1}Si_{9.2}$; $\tau_2+(Ta,V)$, (c) $Ta_{17.5}V_{59.1}Si_{23.4}$; $\tau_1+\tau_2+(Ta_xV_{1-x})_3Si$ and (d) $Ta_{32.7}V_{61.1}Si_{6.2}$; $\tau_2+\tau_3+(Ta,V)$.

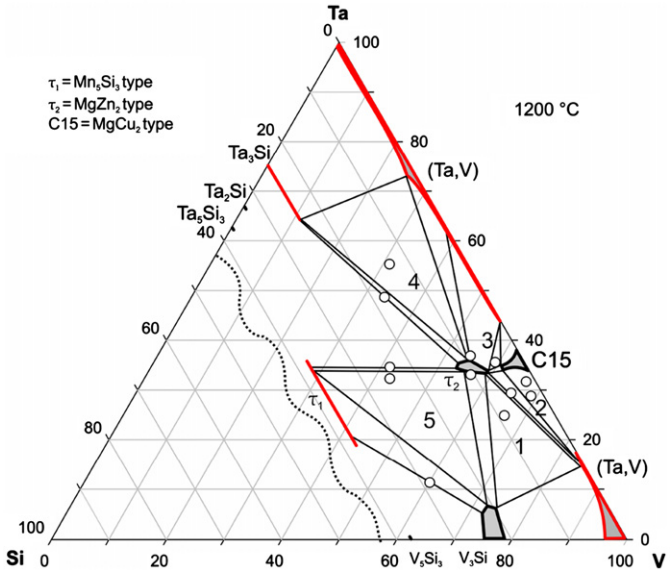

Fig. 9. Isothermal section of the Ta–V–Si system at 1200 °C. Sample location is shown by open circles.

also section "Binary boundary systems"). The partial isothermal section based on our results is shown in Fig. 9. Compositions and lattice parameters of the alloys revealing three-phase equilibria are shown in Table 4. τ_2 has a rather small homogeneity region at 1200 °C as compared to its extent at 1500 °C but τ_2 is still present in equilibrium with τ_1 and $(Ta_xV_{1-x})_3Si$. However, τ_3 is connected with the Ta–V binary and exhibits a solubility of Si up to ~4 at.%. τ_3 is present in equilibrium with (Ta,V) on both sides in contrast to the isothermal section at 1500 °C where a continuous solid solution was observed between Ta and V and τ_3 was observed as truly ternary phase without any connection to the binary Ta–V section.

General Remarks: comparing the phase relations in the system Ta–V–Si–(C) at 1400 °C [4] with our section of Ta–V–Si at 1500 °C we see that small amounts of carbon do not exert a significant influence on the solubility of Ta in V_3Si and of V in Ta_3Si and there is no change for the continuous solid solution $Ta_{1-x}V_xSi_2$. Although the Mn_5Si_3-type solid solution τ_1-$(Ta_xV_{1-x})_5Si_3$, without interstitial atoms in the 2*a* site, shows a remarkably large homogeneity region at 1500 °C, it is confined to the ternary system. But the end members Ta_5Si_3 and V_5Si_3 will be included into this solution under the stabilizing influence of carbon. It is, however, unclear if small amounts of carbon can destabilize the Laves phases or for what other reasons Nowotny et al. [4] did not observe the two Laves phases, which dominate the phase equilibria in the Si-poor region of the carbon free Ta–V–Si system. A thermodynamic evaluation of the Ta–V–Si system will be the task of a forthcoming paper in order to (i) shed more light on the stabilizing influence of silicon on the two Laves phases and to (ii) elucidate the thermodynamic stabilities and phase relations among the three competing structure types Cr_5B_3, Mn_5Si_3, W_5Si_3 along the section Ta_5Si_3–V_5Si_3.

4. Conclusion

Phase relations in the Ta–V–Si system have been evaluated for the isothermal sections at 1500 and 1200 °C revealing three ternary phases: τ_1-$(Ta,V)_5Si_3$ (Mn_5Si_3-type) and the Laves phases τ_2-$Ta(Ta,V,Si)_2$ ($MgZn_2$-type) and τ_3-$Ta(Ta,V,Si)_2$ ($MgCu_2$-type).

Table 4
Data on alloys for three-phase regions in the Ta–V–Si system at 1200 °C.

Three phase regions	Phase	Structure type	Lattice parameters (nm)			Composition (at.%)		
			a	*b*	*c*	Ta	V	Si
τ_2+$(Ta_xV_{1-x})_3Si$ +(Ta,V)	τ_2	$MgZn_2$	0.50293(5)	–	0.82353(9)	33.4	58.6	8.0
(1)[a]	$(Ta_xV_{1-x})_3Si$	Cr_3Si	0.47434(4)	–	–	6.2	74.4	19.4
	(Ta,V)	W	0.31097(1)	–	–	14.5	84.5	1.0
τ_2+C15+(Ta,V)	τ_2	$MgZn_2$	0.50160(2)		0.82446(7)	33.6	59.2	7.2
(2)	C15	$MgCu_2$	0.71299(4)	–	–	33.9	61.4	4.7
	(Ta,V)	W	0.31127(8)	–	–	15.8	83.5	0.7
τ_2+C15+(Ta,V)	τ_2	$MgZn_2$	0.50456(8)		0.82405(8)	34.1	58.8	7.1
(3)	C15	$MgCu_2$	0.71365(8)	–	–	34.9	60.5	4.6
	(Ta,V)	W	0.32179(2)	–	–	53.5	46.4	0.1
τ_2+(Ta,V) +$(Ta_{1-x}V_x)_3Si$	τ_2	$MgZn_2$	0.50161(6)		0.82564(6)	35.6	54.4	9.8
(4)	(Ta,V)	W	0.32636(5)	–	–	72.8	25.2	2.0
	$(Ta_{1-x}V_x)_3Si$	Ti_3P	1.01142(7)	–	0.51323(8)	63.8	11.2	25.0
τ_1+τ_2 +$(Ta_{1-x}V_x)_3Si$	τ_1	Mn_5Si_3	0.73741(9)	–	0.49990(5)	33.8[b]	28.7	37.5
(5)	τ_2	$MgZn_2$	0.50151(4)		0.82527(6)	33.7	52.6	11.7
	$(Ta_xV_{1-x})_3Si$	Cr_3Si	0.47481(4)	–	–	6.8	72.1	21.1

[a] Corresponding no. of triangles shown in isothermal section at 1500 °C in Fig. 7.
[b] Composition of phases evaluated from Figs. 5 and 6.

The crystal structures of the three phases were solved by single crystal diffraction (τ_2) or from X-ray powder diffraction data (τ_1 and τ_3). The homogeneity region at 1200 and 1500 °C obtained for the τ_2-phase does not include the stoichiometric composition Ta_2V_3Si. Although a Laves phase with $MgZn_2$-type does neither exist in the binary Ta–V system at 1500 nor at 1200 °C, the corresponding Laves phase (τ_2-phase) is present in the ternary system at these temperatures documenting a strong stabilizing effect of silicon. A large homogeneity range was found for τ_1-$(Ta_xV_{1-x})_5Si_3$ with Mn_5Si_3-type showing the exchange of Ta and V at a constant Si content. At 1500 °C, the end points of the τ_1-phase solution ($0.082 \le x \le 0.624$) are in equilibrium with $(Ta_{1-x}V_x)_5Si_3$ (Cr_5B_3 type, $0 \le x \le 0.128$) and with $(Ta_xV_{1-x})_5Si_3$ (W_5Si_3 type, $0 \le x \le 0.048$). Rietveld refinements showed the absence of any significant residual electron density in the sites for the octahedral voids in 2*b* (0, 0, 0) excluding interstitial atoms in τ_1-$(Ta_xV_{1-x})_5Si_3$.

Acknowledgements

A.U. Khan is grateful for the continued support by the Higher Education Commission of Pakistan (HEC) under the scholarship scheme "PhD in Natural and Basic Sciences from Austria" and by the Austrian OEAD. Project MSM0021622410 from Ministry of Education of the Czech Republic and project "CEITEC – Central European Institute of Technology" (ED1.1.00/02.0068) from the European Regional Development Fund is thankfully acknowledged by P. Broz. X.-Q.C is grateful for support from the "Hundred Talents Project" of the Chinese Academy of Sciences and from NSFC of China (Grant Numbers: 51074151 and 51174188).

References

[1] P. Fernandez, A.M. Lancha, J. Lapena,, M. Hernandez-Mayoral, Fusion Engineering and Design 58-59 (2001) 787–792.
[2] A.-A.F. Tavassoli, Journal of Nuclear Materials 302 (2002) 73–88.
[3] M.V. Nevitt, in: P.A. Beck (Ed.), Electronic Structure and Alloy Chemistry of the Transition Elements, Willey-Interscience, New York, 1963.
[4] H. Nowotny, B. Lux, H. Kudielka, Monatshefte für Chemie 87 (3) (1956) 447–470.
[5] H. Nowotny, E. Dimakopoulou, H. Kudielka, Monatshefte für Chemie 88 (1957) 180–192.
[6] J.F. Smith, in: Second Edition,in: T.B. Massalski (Ed.), Binary Alloy Phase Diagrams, 3, ASM International, Materials Park, Ohio, 1990, pp. 3374–3377.
[7] J.J. English, Si-Ta-V phase diagram, in: J.J. English (Ed.), Binary and Ternary Phase Diagrams of Columbium, Molybdenum, Tantalum and Tungsten, AD-407987, DMIC Report 183 from February 7, 1963 (Supplement to DMIC Report 152), vol. 1, Defense Documentation Center for Scientific and Technical Information, Cameron Station, Alexandria, Virginia, USA, 1963, pp. 1–127.
[8] J.J. English, Ta-V-Si Phase Diagram, in: P. Villars, A. Prince, H. Okamoto (Eds.), Handbook of Ternary Alloy Phase Diagrams, ASM International, Materials Park, OH, 1995, p.13583.
[9] E. Ganglberger, H. Nowotny, F. Benesovsky, Monatshefte für Chemie 96 (5) (1965) 1658–1659.
[10] R.C. Mittal, S.K. Si, K.P. Gupta, Journal of Less Common Metals 60 (1978) 75–82.
[11] J. Steinmetz, B. Roques, C.R. Academy, Science Paris, Series C 283 (1976) 633–635.
[12] J. Steinmetz, B. Roques, Journal of Less-Common Metals 52 (1977) 247–258.
[13] N.Y. Alekseyevskiy, N.Y. Ageyev, V.F. Shamray (Eds.), Physics of Metals and Metallography, translated from Fizika Metallov, Metallovedenie, 43, 1977, pp. 42–48.
[14] Nonius Kappa CCD, Program Package COLLECT, DENZO, SCALEPACK, SORTAV, Nonius Delft, The Netherlands.
[15] G.M. Sheldrick, SHELXL-97, Program for crystal structure refinement, University of Göttingen, Germany; Windows version by McArdle, Natl Univ., Ireland, Galway, 1997.
[16] J.F. Smith, O.N. Carlson, in: T.B. Massalski (Ed.), Binary Alloy Phase Diagrams, vol. 3, second ed., ASM International, Materials Park, Ohio, 1990, pp. 3364–3366; for details see: J.F. Smith, O.N. Carlson, The Ta-V system, Bull. Alloy Phase Diagrams 4 (3) (1983) 284–289.
[17] A.P. Nefedov, E.M. Sokolovskaya, A.T. Grigor'ev, V.I. Chechernikov, I.G. Sokolova, L.S. Guzei, Vestnik Moskovskogo Universiteta, Seriya 2: Khimiya 5 (1965) 42–47.
[18] A.P. Nefedov, E.M. Sokolovskaya, A.T. Grigor'ev, I.G. Sokolova, N.A. Nedumov (Eds.), Russian Journal of Inorganic Chemistry, Translated from Zhurnal Neorganichekoi Khimii, 9, 1964, pp. 486–489.
[19] V.N. Yeremenko, L.A. Tretyachenko, Z.P. Golubenko, Dopovidi Akademii Nauk Ukrainskoi RSR (1962), pp. 192-195.
[20] E. Rudy, Compendium of Phase Diagram Data, published as Tech. Rep. AD 689, 843 (1969), available from NTIS as document no. AFML-TR-65-2, part V.
[21] E.M. Savitskii, J.V. Efimov, Monatshefte für Chemie 103 (1972) 270–287.
[22] J. Pavlu, J. Vrestal, X.–Q. Chen, P. Rogl, CALPHAD: Computer Coupling of Phase Diagrams and Thermochemistry 35 (2011) 103–108.
[23] C.A. Danon, C. Servant, Journal of Alloys and Compounds 366 (2004) 191–200.
[24] Z. Guo, W. Yuan, Y. Sun, Z. Cai, Z. Qiao, Journal of Phase Equilibria and Diffusion 30 (5) (2009) 564–570.

[25] C. Zhang, Y. Du, W. Xiong, H. Xu, P. Nash, Y. Ouyang, R. Hu, Computer Coupling of Phase Diagrams and Thermochemistry 32 (2008) 320–325.
[26] H. Okamoto, Journal of Phase Equilibria and Diffusion 31 (4) (2010) 409–410.
[27] J. Hallais, J.P. Senateur, R. Fruchart, C.R. Academy, Science Paris, Serie C 264 (1967) 1947–1950.
[28] P. Spinat, R. Fruchart, P. Herpin, Bulletin Société Français de Minéralogie et de Cristallographie 93 (1970) 23–36.
[29] J. Hallais, Ann. Chim 6 (1971) 321–330.
[30] V.N. Eremenko, L.A. Tret'yachenko, R.I. Yakhimovich, Russian Journal of Inorganic Chemistry, translated from Zhurnal Neorganicheskoi Khimii 5 (1960) 1110–1112.
[31] H.A.C.M. Bruning, Philips Research Reports 22 (4) (1967) 349–354.
[32] H. Müller, K. Weymann, Journal of the Less-Common Metals 119 (1986) 115–126.
[33] Y.A. Kocherzhinskii, O.C. Kulik, E.A. Shishkin (Eds.), Doklady Chemistry, translated from Doklady Akademii Nauk SSSR, 261, 1981, pp. 464–465.
[34] J.C. Lasjaunias, O. Laborde, U. Gottlieb, R. Madar, O. Thomas, Journal of Low Temperature Physics 92 (1993) 335–351.
[35] K. Kanematsu, Transactions of the Japan Institute of Metals 27 (1986) 225–232.
[36] M.A. Rykova, A.V. Sabirzyanov, P.V. Gel'd (Eds.), Inorganic Materials, translated from Izvestiya Akademii Nauk SSSR, Neorganicheskie Materialy, 10, 1974, pp. 122–123.
[37] L.M. Gelato, E. Parthé, Journal of Applied Crystallography 20 (1987) 139–143.
[38] H. Nowotny, E. Laube, Planseeberichte für Pulvermetallurgie 9 (1961) 54–59.
[39] H. Nowotny, B. Lux, H. Kudielka, Monatshefte für Chemie 87 (1956) 447–470.
[40] H. Nowotny, H. Schachner, R. Kieffer, F. Benesovsky, Monatshefte für Chemie 84 (1) (1953) 1–12.
[41] E. Parthé, H. Nowotny, H. Schmid, Monatshefte für Chemie 86 (1955) 385–396.
[42] P. Villars, K. Cenzual, Pearson's Crystal Data, ASM International, Ohio, USA, Release 2010/11.